



ARTICLE

Iptakalim improves cerebral microcirculation in mice after ischemic stroke by inhibiting pericyte contraction

Ruo-bing Guo¹, Yin-feng Dong², Zhi Yin³, Zhen-yu Cai¹, Jin Yang¹, Juan Ji¹, Yu-qin Sun¹, Xin-xin Huang³, Teng-fei Xue¹, Hong Cheng³, Xi-qiao Zhou² and Xiu-lan Sun^{1,2}

Pericytes are present tight around the intervals of capillaries, play an essential role in stabilizing the blood–brain barrier, regulating blood flow and immunomodulation, and persistent contraction of pericytes eventually leads to impaired blood flow and poor clinical outcomes in ischemic stroke. We previously show that iptakalim, an ATP-sensitive potassium (K-ATP) channel opener, exerts protective effects in neurons, and glia against ischemia-induced injury. In this study we investigated the impacts of iptakalim on pericytes contraction in stroke. Mice were subjected to cerebral artery occlusion (MCAO), then administered iptakalim (10 mg/kg, ip). We showed that iptakalim administration significantly promoted recovery of cerebral blood flow after cerebral ischemia and reperfusion. Furthermore, we found that iptakalim significantly inhibited pericytes contraction, decreased the number of obstructed capillaries, and improved cerebral microcirculation. Using a collagen gel contraction assay, we demonstrated that cultured pericytes subjected to oxygen-glucose deprivation (OGD) consistently contracted from 3 h till 24 h during reoxygenation, whereas iptakalim treatment (10 μ M) notably restrained pericyte contraction from 6 h during reoxygenation. We further showed that iptakalim treatment promoted K-ATP channel opening via suppressing SUR2/EPAC1 complex formation. Consequently, it reduced calcium influx and ET-1 release. Taken together, our results demonstrate that iptakalim, targeted K-ATP channels, can improve microvascular disturbance by inhibiting pericyte contraction after ischemic stroke. Our work reveals that iptakalim might be developed as a promising pericyte regulator for treatment of stroke.

Keywords: stroke; cerebral ischemia; iptakalim; ATP-sensitive potassium channels; pericytes; microcirculation

Acta Pharmacologica Sinica (2022) 43:1349–1359; <https://doi.org/10.1038/s41401-021-00784-4>

INTRODUCTION

Ischemic stroke is the second leading cause of death and the first leading cause of adult disability [1]. Restoring cerebral blood flow (CBF) as early as possible is critical for treating ischemic stroke [2]. Currently, intravenous thrombolysis or endovascular thrombectomy is an effective strategy; however, it is available for <5% of patients, and 50% of them have a poor prognosis. A growing number of studies have indicated that the primary cause is the “no-reflow” phenomenon [3, 4], defined as impaired recanalization during reperfusion. No-reflow becomes more serious with extended periods of ischemia [5], and likely decreases CBF and increases the infarct size. Clinical trials have shown that no-reflow treatment can extend the therapeutic window to 24 h after stroke [6]. Therapies targeting no-reflow areas result in improved stroke outcomes [7]. No-reflow can occur within a window of brain parenchymal viability [8]. The no-reflow phenomenon was previously attributed to endothelial swelling and astrocytic end-feet compression. In recent years, accumulating studies have demonstrated that pericyte contraction can severely impede erythrocyte reflux and trap fibrin, platelets, and white blood cells in capillaries [9]. Pericytes tightly

encircle capillaries, and play an essential role in stabilizing the blood–brain barrier, regulating blood flow, and immunomodulation [10]. The persistent contraction of pericytes eventually leads to impaired blood flow and poor clinical outcomes. Thus, there is an urgent need to develop a regulator of pericytes to restore blood flow after ischemic stroke.

Iptakalim (IPT) is a novel ATP-sensitive potassium channel (K-ATP) opener that was independently developed in China. It has high selectivity for the sulphonylurea receptor 2B (SUR2B)/Kir6.1 subtype [11] but does not exhibit the adverse side effects associated with other nonspecific K⁺ channel openers. Moreover, it causes arteriolar vasodilatation without effects on capillaries or large arteries [12]. Our previous studies suggested that IPT protects neurons, astrocytes, and microglia against ischemic injuries [13–15]. A recent study confirmed the high gene expression of ATP Binding Cassette Subfamily C Member 9 (ABCC9) and Potassium Inwardly Rectifying Channel Subfamily J Member 8 (KCNJ8) encoding SUR2 and Kir6.1, respectively, in pericytes [16]. Therefore, it is worth determining whether IPT can regulate pericyte contraction and improve microcirculation after ischemic stroke.

¹Neuroprotective Drug Discovery Key Laboratory, Jiangsu Key Laboratory of Neurodegeneration, Nanjing Medical University, Nanjing 211166, China; ²Nanjing University of Chinese Medicine, The Affiliated Hospital of Nanjing University of Chinese Medicine, Nanjing 210029, China and ³The First Affiliated Hospital of Nanjing Medical University, Nanjing 210029, China

Correspondence: Xiu-lan Sun (xiulans@njmu.edu.cn) or Hong Cheng (13815877695@126.com) or Xi-qiao Zhou (zhouxiqiao@njucm.edu.cn)
These authors contributed equally: Ruo-bing Guo, Yin-feng Dong

Received: 27 July 2021 Accepted: 23 September 2021

Published online: 25 October 2021

In this study, we investigated the regulatory effects and mechanisms of IPT on pericyte contraction in vitro and in vivo studies. We found that IPT inhibited SUR2/exchange protein directly activated by cAMP 1 (EPAC1) complex formation, promoted SUR2/Kir6.1 K-ATP channel opening, and reduced endothelin-1 (ET-1) secretion in pericytes. Our novel findings reveal that IPT can inhibit pericyte contraction and improve capillary blood flow after cerebral ischemia–reperfusion.

MATERIALS AND METHODS

Animals and treatments

Male C57BL/6j mice aged 8–10 weeks (22 ± 2) g were obtained from Nanjing Medical University (Jiangsu, China). They were maintained in the Animal Resource Center of the Faculty of Medicine, and had free access to food and water. The room temperature was maintained at 22 ± 2 °C with a 12:12 h light: dark cycle. The mice were randomly divided into three groups: sham, middle cerebral artery occlusion (MCAO), and MCAO + IPT groups. At 1 h after MCAO, the MCAO + IPT group was administered IPT (10 mg/kg; provided by Prof. Hai Wang, Institute of Pharmacology and Toxicology, Academy of Military Medical Sciences, Beijing, China) by intraperitoneal (IP) injection, and the other groups were administered saline. IPT was dissolved in saline, and the dosage (10 mg/kg) was based on our previous studies [14, 17].

MCAO model

To establish the MCAO model, the mice were anesthetized with sodium pentobarbital (40 mg/kg) by IP injection, and the proximal MCA was occluded for 1 h with a 6–0 silicon-coated nylon suture as previously described [18]. The mice were placed on a heating blanket during the surgical procedure, and the body temperature was maintained at 37 ± 0.5 °C by a rectal probe. All animal experiments were approved by the review committee of Nanjing Medical University and complied with institutional guidelines (No. IACUC-1801010).

2,3,5-Triphenyltetrazolium chloride staining

To assess the infarct volume, we performed 2,3,5-triphenyltetrazolium chloride (TTC; Sigma, St. Louis, MO, USA) staining. Brains were sliced into 1 mm coronal sections, incubated in 2% TTC for 3 min at 37 °C in the dark, and fixed in 4% paraformaldehyde (PFA) overnight. The area of infarction (“direct stroke area”) was quantified, and the infarct volume was calculated using Image-Pro Plus 5.1 software.

Neurological score

The NeuroScore is commonly used to assess neurological disorders [19] as follows: 0, normal motor function; 1, flexion of the torso and contralateral forelimb after lifting the animal by the tail; 2, circling to the ipsilateral side, but normal posture at rest; 3, circling to the ipsilateral side; 4, rolling to the ipsilateral side; and 5, leaning to the ipsilateral side at rest (no spontaneous motor activity).

Laser speckle imaging

Laser speckle imaging (LSI) was done using the moorFLPI blood flow imager, and the exposure time was set at 2 ms. A 775 nm laser was used to illuminate the pial microcirculation, and laser speckle images were acquired using a 568×760 pixel grayscale charge-coupled device camera at a sampling rate of 1 Hz. Using the pixel window (5×5) to calculate the speckle contrast, the maximum image resolution was $5 \mu\text{m}/\text{pixel}$. The moorFLPI-2 translates the speckle contrast value into a relative perfusion unit, displaying blood flow velocity and the number of red blood cells. Pseudo-color images with perfusion scaled from blue (low perfusion) to red (high perfusion) were obtained. LSI recordings were performed at baseline, after 5 min of ischemia, and after

10, 20, 30, and 45 min and 1, 2, 3, 4, 6, 8, 10, and 12 h of reperfusion. Imaging processing and quantification were done using moorFLPI-2 research software (Moor Instruments Inc., Wilmington, DE, USA).

Multimodal optical imaging

The custom-built multimodal optical imaging platform (MIP) consisted of multi-wavelength spectral, fluorescence imaging, and LSI modules (MW-LSI) integrated with three-dimensional optical coherence tomography. For MW-LSI, high-brightness light-emitting diodes (LEDs) ($\lambda = 568$ nm) were used for total hemoglobin imaging. The back-reflected light was collected using a modified zoom microscope (AZ100; Nikon, Tokyo, Japan) and acquired by a 16-bit sCMOS camera at 80 or 16 fps. Imaging processing and quantitative analyses were done as previously described [20].

Sample processing

At the end of reperfusion, mice were euthanized with an overdose of pentobarbital sodium and transcardially perfused with saline (100 mL) followed by 4% PFA (100 mL). Then 10 mL of 5% gelatin solution (G2625; Sigma) containing Texas Red (Merck Millipore, Burlington, MA, USA) was perfused in the coronary microvasculature. Finally, the whole brain tissues were separated and fixed overnight in 4% PFA, and a $50 \mu\text{m}$ coronal section of brain tissues was used for immunofluorescence staining. The analysis of images was referred to by Attwell [21].

Immunofluorescence staining

Immunofluorescence was performed as previously described [22]. Pericytes were labeled with anti-neuron-gial antigen 2 (NG2) (1:200, AB5320; Merck Millipore) and the capillary basement membrane was labeled with isolectin B4 conjugated to Alexa Fluor 647 (I32450; Molecular Probes, Eugene, OR, USA) or Texas Red (Merck Millipore). Z-stacks for cell counting were acquired by laser scanning microscopy (LSM 700; Zeiss, Wetzlar, Germany). The intersoma distance of pericytes was detected as the distance between pairs of pericytes surrounding the capillaries.

Detection of trapped erythrocytes

Under anesthesia, the mice were transcardially perfused with 100 mL heparinized saline ($10 \text{ IU} \cdot \text{mL}^{-1}$) followed by 4% PFA. After euthanasia, the whole brain was removed and kept in PFA for 24 h. Then the brain tissues were dehydrated in graded ethanol and embedded in paraffin, after which $6 \mu\text{m}$ brain slices were deparaffinized overnight and gradually hydrated in ethanol. The slices were treated with 0.2% sodium borohydride for 30 min and then rinsed with phosphate-buffered saline (PBS) for 10 min [23].

Primary pericyte culture

Pericyte isolation was done according to the protocol by Tigges et al. [24]. The mice were euthanized by overdose of pentobarbital sodium, and the brain tissues were rapidly removed and placed in cold Minimum Essential Medium (MEM). The olfactory bulb, cerebellum, and medulla were dissected, and the remaining tissues were thoroughly minced, washed with MEM, and centrifuged at 1200 r/min for 5 min. Then the suspension was digested with enzymatic solution (Solarbio, Beijing, China) containing 30 U/mL papain and $40 \mu\text{g}/\text{mL}$ DNase I in Earle's Balanced Salt Solution for 70 min at 37 °C, homogenized, and filtered 10 times through 19- and 21-gauge needles. Then it was mixed with 22% bovine serum albumin (BSA) and centrifuged at 4000 r/min for 10 min. After removing the cell supernatant, the pellet was resuspended in 5 mL endothelial cell growth medium (ECGM) (Cat. No. 1001; ScienCell Research Laboratories, Inc., Carlsbad, CA, USA) and centrifuged at 1200 r/min for 5 min. Finally, the cell pellets were resuspended in ECGM and plated in a 6-well

Collagen I-coated plate (0.02% solution; Sigma). After 20 h, cells were washed three times with PBS and cultured in fresh ECGM. The cell culture medium was changed every 3 days. After 7–9 days, the cells reached confluency and were harvested with trypsin and transferred to fresh collagen-coated 6-well plates. During the first two passages, the cells were cultured in ECGM. After the third passage, cells were cultured in pericyte medium (Cat. No. 1201; ScienCell) containing 2% fetal bovine serum (FBS). The cells were passaged 4–7 times, and the purity of the pericytes was determined by immunofluorescence staining.

Oxygen-glucose deprivation model

An oxygen-glucose deprivation/reoxygenation (OGD/R) model was established according to our previous study [25]. Briefly, the pericytes were washed and incubated in glucose-free Dulbecco's modified Eagle's medium (DMEM) (Gibco, Gaithersburg, MD, USA) without FBS, and then placed in an anaerobic chamber (Mitsubishi Gas Chemical Company, Tokyo, Japan). At 3 h after OGD, cells were replaced with standard medium containing 10% FBS and returned to the normoxic incubator (37 °C, 5% CO₂). The control group was treated similarly but not exposed to OGD.

Collagen gel contraction assay

The collagen gel contraction assay was conducted to study cell-induced contractions of the extracellular matrix. Briefly, 90 µL rat tail collagen type I (0.5 mg/mL; Solebo Inc.) was mixed with 12 µL of 0.1 M NaOH in an Eppendorf tube. Then the pericytes were harvested, added (1×10^5 cells/148 µL) to the mixture, and seeded in a 24-well plate (250 µL solution/well). This process was conducted quickly on ice. The 24-well plate was placed in the cell incubator for 1 h, and then 500 mL pericyte medium containing 2% FBS was added to each well. Finally, the 24-well plate was incubated for 12 to 24 h. Before OGD, gels in each well were captured by a camera (OnePlus 5T, China) at 0 h, replaced with glucose-free DMEM, and kept in hypoxic bags (2.5 L Anaero Pack, Japan) for 3 h. Then the glucose-free DMEM was removed and replaced with standard pericyte medium. At 6 and 24 h of reoxygenation, each gel was captured; the area at 0 h was set as the control.

Intracellular calcium detection

Pericytes were cultured in 48-well plates, and cells were incubated with Fluo 4-AM fluorescent probe diluted in 100 µL calcium-free Krebs' buffer (F14201; Thermo Fisher Scientific, Waltham, MA, USA) at 37 °C for 30 min. Then cells were gently washed once with Krebs' buffer and returned to the original medium. At 0 and 3 h of OGD and 2, 4, and 6 h of reoxygenation, intracellular calcium levels were measured using the multimode microplate reader (Biotek, Winooski, VT, USA) at excitation and emission wavelengths of 488 and 515 nm, respectively.

Co-immunoprecipitation

Co-immunoprecipitation was performed according to previous study [22]. Briefly, pericytes were washed twice with 0.1 M PBS and lysed in NP-40 lysis buffer. The cell suspension was centrifuged at 12,000 × *g* for 15 min, and the supernatant was transferred to another centrifuge tube. The protein sample was quantified; one portion of the sample was incubated with EPAC1 primary antibody (2 µg/500 µg) and rotated at 4 °C overnight, and the other portion was boiled at 100 °C for 10 min and mixed with 1× loading buffer. Protein A and G beads (100 µL/mL cell lysate) were added to the sample and rotated at 4 °C for 4 h. Then the mixture was centrifuged at 12000 × *g* for 5 min. After removing the supernatant, beads were preserved and washed three times (10 min/time) with 600 µL RIPA supplemented with PMSF. Finally, the sample was centrifuged at 12000 × *g* for 15 min, and the supernatant was mixed with 1× loading buffer and stored at –80 °C.

Western blotting

Pericytes were lysed in RIPA buffer (50 mM Tris, pH 8.0, 150 mM NaCl, 0.1% sodium dodecyl sulfate [SDS], 1.0% NP-40, 0.5% sodium deoxycholate plus 1× protease inhibitor cocktail). Cytoplasmic and nuclear proteins were extracted with a protein extraction kit (Beyotime, Shanghai, China) and quantified according to the manufacturer's instructions. Proteins were resolved by SDS-polyacrylamide gel electrophoresis and electrotransferred to PVDF membranes. The membranes were blocked in 5% BSA for 1 h at room temperature and then incubated overnight at 4 °C with the following primary antibodies: rabbit anti-GAPDH (1:1000, 5174S; Cell Signaling Technology [CST], Danvers, MA, USA), rabbit anti-calcium/calmodulin-dependent protein kinase II delta (CaMKIIδ) (1:1000, #ab181052; Abcam, Cambridge, MA, USA), rabbit anti-phosphorylated CaMKII (p-CaMKII) (1:1000, #12716S; CST), rabbit anti-EPAC1 (1:1000, #ab109415; Abcam), and mouse anti-ABCC9 (1:500, #ab174629; Abcam). After washing three times, the membranes were incubated with horseradish peroxidase-conjugated secondary antibody for 1 h at room temperature. The immunoblots were scanned and analyzed using the Omega 16ic Chemiluminescence Imaging System (Ultra-Lum, Claremont, CA, USA) and quantified using ImageJ software.

Enzyme-linked immunosorbent assay

Cell supernatants were centrifuged at 3000 r/min for 10 min. The content of ET-1 in the cell supernatants was detected using an enzyme-linked immunosorbent kit (R&D Systems, Cambridge, UK) according to the manufacturer's instructions.

Quantitative PCR

Total RNA was isolated from the ipsilateral striatum using the miRNeasy Mini Kit (Qiagen, Hilden, Germany). Then it was reverse transcribed using a cDNA synthesis kit (Life Technologies,

Table 1. The primers for PCR amplification.

| Target gene | Forward primer sequence (5' to 3') | Reverse primer sequence (5' to 3') |
|-------------|------------------------------------|------------------------------------|
| GAPDH | TGTGTCCGTCGTGGATCTGA | TTGCTGTTGAAGTCGCAGGAG |
| Kir6.1 | TTGAACCACACGGGTCATCAT | GCAGGTGCTATTTGCTTGGTTAG |
| Kir6.2 | GTAGGGGACCTCCGAAAGAG | CAGGAAGATGCCGTTACCAC |
| SUR1 | GTTTTATAAGAGTAGTTGGAAGG | TTATTAACAAACACCTTAATCCACCC |
| SUR2 | CATGCCTGTTTCAGATCATAATG | AACACTGATGATGGCTTTG |
| CAMKIIα | TATCCGCATCACTCAGTACCTG | GAAGTGGACGATCTGCCATTT |
| CAMKIIβ | GCACGTCATTGGCGAGGAT | ACGGGTCTCTTCGGACTGG |
| CAMKIIγ | CGACTACCAGCTTTTCGAGG | GCCTCTCGTTCTAGTTTCTGATG |
| CAMKIIδ | GCTAGGGACCATCAGAAACTG | GTCTTCAAACAGTTCGCCAC |
| EPAC1 | AGAGATGCCCGACTTAGCAA | TTGGTCTGAGGAGATACG |
| EPAC2 | ATAAAAGGCCGTTGGAGCGA | GCCAGGACAGCATACCAGTT |

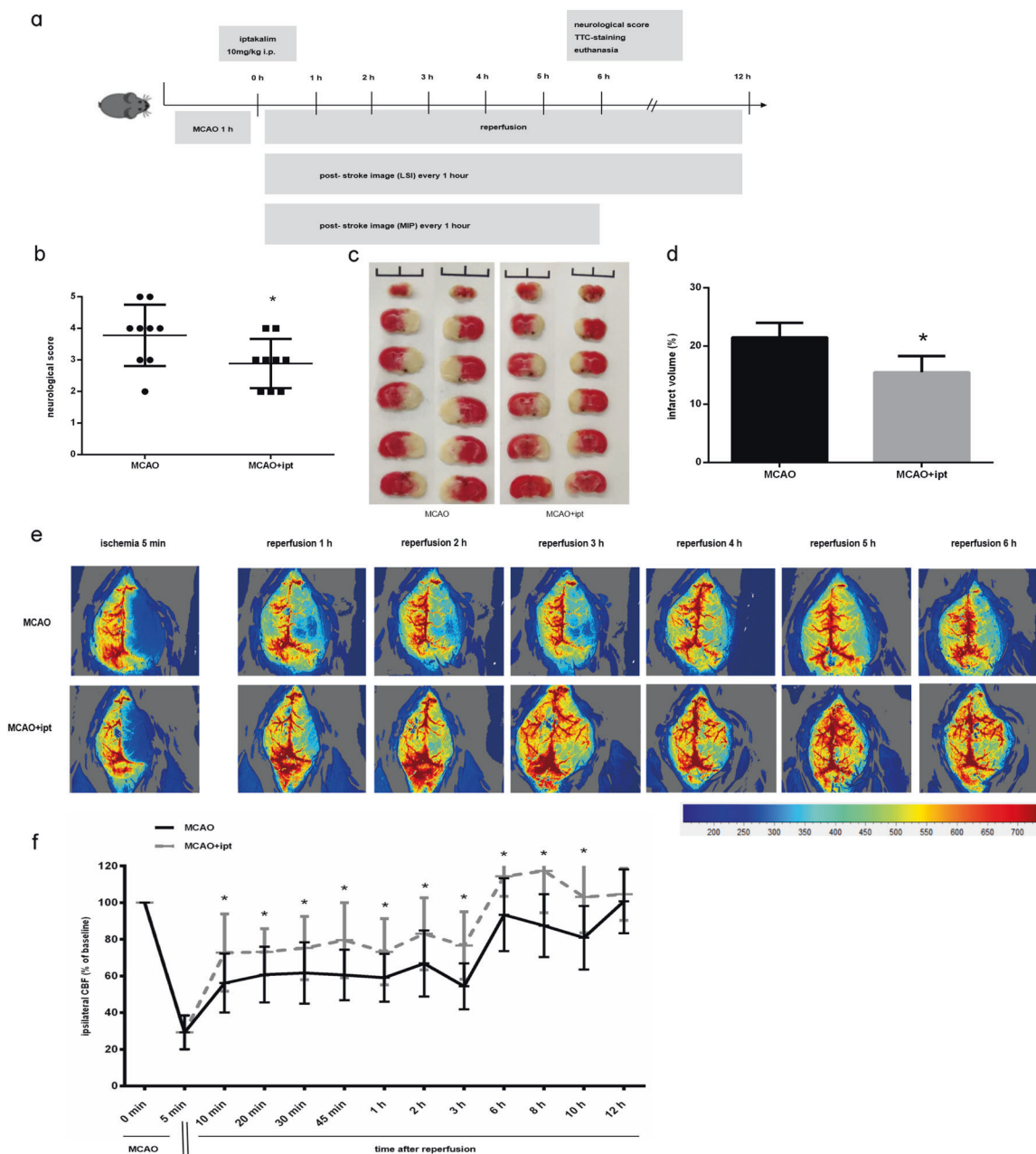


Fig. 1 Iptakalim treatment significantly alleviates ischemic brain injury and promotes recovery of cerebral blood flow. **a** Schematic diagram of experimental design. **b** Neurological score. **c** Representative TTC-staining brain slices. **d** Total volume of the ischemic lesion in the ipsilateral hemisphere was assessed at post-MCAO 6 h. Data are presented as mean \pm SEM, $n = 8$, * $P < 0.05$ vs. MCAO group. **e** The time course of representative LSF images and **(f)** average CBF in the ipsilateral brain. Red color, high CBF; blue color, low CBF. Data are presented as mean \pm SEM, $n = 6$, * $P < 0.05$ vs. MCAO group .

Carlsbad, CA, USA). Crossing threshold values were set at 2.0 and normalized to the housekeeping gene GAPDH. The relative gene expression was shown as the fold change ($\Delta\Delta Ct$) and normalized to the control group. Primers for each index are listed in Table 1.

Statistical analysis

Data are presented as the mean \pm standard error of the mean. Unless stated otherwise, all quantitative statistical assessments were performed in a blinded manner. One-way analysis of variance (ANOVA) followed by the Student–Newman–Keuls test was used for comparisons of three or more groups. Data shown in Figs. 1f, 2a, 4d, e were analyzed by two-way repeated measures

ANOVA followed by the Bonferroni *post hoc* test. If the assumption of sphericity was violated with $P < 0.05$, we applied the Greenhouse–Geisser procedure to correct the degrees of freedom of the F -distribution. $P < 0.05$ was considered statistically significant.

RESULTS

IPT treatment significantly alleviates ischemic brain injury and promotes recovery of CBF

To assess the protective effects of IPT, we determined the neurological score and observed the infarct size. The experimental design is shown in Fig. 1a. Compared with the MCAO group,

treatment with IPT (10 mg/kg) significantly decreased the neurological score (Fig. 1b). TTC-staining results showed that the infarct size of the MCAO group was $21.5\% \pm 2.5\%$, which was decreased to $15.5\% \pm 2.8\%$ with IPT treatment (Fig. 1d). To determine the potential therapeutic benefits of promoting recovery of CBF, we used laser speckle Doppler flowmetry to evaluate CBF changes during ischemia and reperfusion. After 5 min of brain ischemia, CBF decreased by 70% in the ipsilateral brain (Fig. 1e) and rapidly recovered from reperfusion of 10 min to 12 h (Fig. 1f). By contrast, IPT treatment (72.71% of baseline) led to better recovery of CBF than the MCAO group (56.14% of baseline) from reperfusion of 10 min (Fig. 1f). At 6 h post-ischemia, the IPT treatment group almost recovered to baseline (Fig. 1e). These results indicated that IPT treatment promoted recovery of CBF, decreased infarct size, and alleviated neurological impairment after cerebral ischemia–reperfusion in mice.

IPT treatment improves cerebral microcirculatory dysfunction after cerebral ischemia–reperfusion in mice

Microcirculatory perfusion determines the primary outcome of ischemic stroke [26]. Thus, we observed microcirculatory blood flow in the cortical region of interest using the multimodal optical system imaging within 6 h of reperfusion. The results showed that microcirculatory blood flow significantly decreased from 2 to 6 h after reperfusion, while IPT treatment prevented the decrease in CBF (Fig. 2a). Likewise, the number of capillaries was significantly decreased at 6 h after reperfusion, while IPT treatment partially reversed this trend (Fig. 2b). To further analyze the restoration of microcirculatory dysfunction at the ipsilateral site, we measured the diameter and number of red blood cells trapped in the microvascular network at 6 h after reperfusion. Compared to baseline, there was some microvascular rupture and hemorrhage (marked with a red asterisk) at 1 h after ischemia. After 6 h of reperfusion, a large area of the microvascular ruptured or disappeared in the MCAO group with a significant decrease in diameter, while treatment with IPT partially reversed this effect (Fig. 2c). Capsular contracture leads to lots of trapped erythrocytes, which can be labeled by fluorescent sodium borohydride (NaBH_4) [8]. As shown in Fig. 2d, a significant number of NaBH_4 -positive erythrocytes in the core region ($57 \pm 6/\text{mm}^2$) and penumbra ($80 \pm 14/\text{mm}^2$) in the MCAO group were present after 6 h of reperfusion, but IPT treatment significantly reduced the number of erythrocytes trapped in the core region ($44 \pm 1/\text{mm}^2$) and penumbra ($34 \pm 6/\text{mm}^2$). Collectively, these results indicate that IPT can improve microcirculatory dysfunction by increasing the number of cells in the microvascular and its diameter, which can prevent microcirculatory dysfunction after cerebral ischemia–reperfusion.

The capillary contraction led to lots of trapped erythrocytes, which could be labeled by fluorescent NaBH_4 [8]. As shown in Fig. 2d, a significant number of NaBH_4 -positive erythrocytes in the core region ($57 \pm 6/\text{mm}^2$) and penumbra ($80 \pm 14/\text{mm}^2$) in the MCAO group after 6 h of reperfusion, but iptakalim treatment significantly reduced the number of erythrocytes trapped in the core region ($44 \pm 1/\text{mm}^2$) and penumbra ($34 \pm 6/\text{mm}^2$). Collectively, these results indicated that iptakalim could improve microcirculatory disorder by increasing the number of microvascular and the diameter, which could prevent microcirculatory disorder after cerebral ischemia and reperfusion.

IPT treatment dilates capillaries by inhibiting the contraction of surrounding pericytes

The main reason for no-reflow after cerebral ischemia–reperfusion is microcirculatory dysfunction caused by pericyte contraction. Pericytes are mainly distributed around the capillaries, which are approximately less than $10 \mu\text{m}$ in diameter. To show the relationship between pericytes and capillaries, Texas Red dextran mixed with gelatin solution was perfused in the blood vessels and co-

labeled with pericytes (NG2-positive cells). As shown in Fig. 3a, compared to the sham group, there was reduced pericyte coverage. In addition, many more Texas Red dextran-labeled blood vessels were blurred and discontinuous with subtle breaks in the MCAO group, whereas the red fluorescent blood vessels were intact with fewer breaks in the IPT treatment group. We further analyzed the diameter of blood vessels surrounding the somata of pericytes and found that the mean diameter was about $7.8 \mu\text{m}$ in the MCAO group and $8.3 \mu\text{m}$ in the IPT group (Fig. 3b).

Furthermore, compared with the MCAO group, the intensity of Texas Red dextran–gelatin was also significantly increased in the IPT treatment group, especially at a distance of $10 \mu\text{m}$ from the vascular obstruction site (Fig. 3c), as the processes of pericytes are $<10 \mu\text{m}$ away from each side of the soma [27]. To determine whether pericyte contraction led to a decrease in the diameter of capillaries after ischemia–reperfusion, we measured the diameter of the Texas Red dextran–gelatin-labeled vessels $10 \mu\text{m}$ upstream of the soma. In the MCAO group, the diameter of the soma was 0.705 ± 0.012 , which was increased to 0.813 ± 0.034 with IPT treatment (Fig. 3d). We also observed the area of capillaries covered by pericytes by analyzing NG2- and Texas Red-labeled pericytes. As shown in Fig. 3e, compared with the sham group, the area was significantly decreased by 56% in the MCAO group compared to only 71.9% with IPT treatment. These results suggest that IPT treatment can dilate capillaries by inhibiting pericyte contraction after cerebral ischemia–reperfusion.

IPT treatment inhibits pericyte contraction by reducing SUR2/EPAC1 complex formation, intracellular calcium levels, and ET-1 secretion

IPT mainly acts on SUR subunits and SUR1 can directly bind to EPAC2 in the SUR1/EPAC2 complex, which affects the opening of Kir6.2/SUR1 channels [28]. We detected high mRNA expression of Kir6.1, SUR2, and EPAC1 in pericytes (Supplementary Fig. 1). Further investigations revealed that EPAC1 directly bound to the SUR2 subunit to form complexes in pericytes after OGD/R, while IPT treatment ($10 \mu\text{M}$) reduced SUR2/EPAC1 complex formation (Fig. 4b). To confirm the role of EPAC1, we used the EPAC1-selective agonist (007AM) to pretreat cells. The results showed that OGD/R led to a significant decrease in cell viability, while pretreatment with 007AM inhibited the protective effect of IPT (Fig. 4f). Furthermore, compared to the control group, OGD/R induced the upregulation of phosphorylated CAMKII/CAMKII δ , which was significantly decreased by IPT treatment; pretreatment with 007AM partially inhibited the effect of IPT (Fig. 4c). The intensity of intracellular calcium fluorescence significantly increased over time after OGD/R. IPT treatment reversed this increase in intracellular calcium, and pretreatment with 007AM partially reversed the effect of IPT (Fig. 4d). The collagen gel contraction assay showed that pericytes contracted from 6 to 24 h after reoxygenation. IPT treatment inhibited pericyte contraction, and the effect of IPT was reversed by 007AM pretreatment (Fig. 4e). ET signaling plays a vital role in regulating calcium influx and intracellular calcium homeostasis, and pericyte contraction is mainly mediated by ET signaling [29]. We found that ET-1 level was significantly increased after OGD/R, which was reduced by IPT; 007AM pretreatment partially reversed the effect of IPT (Fig. 4g). These data suggest that IPT opens the K-ATP channels by inhibiting SUR2/EPAC1 complex formation, and reducing intracellular calcium and ET-1 secretion, thus inhibiting pericyte contraction (Fig. 5).

DISCUSSION

The present findings demonstrated that IPT treatment can improve microcirculation by preventing pericyte contraction. IPT regulated pericyte contraction by reducing SUR2/EPAC1 complex formation and opening the K-ATP channel, thus reducing

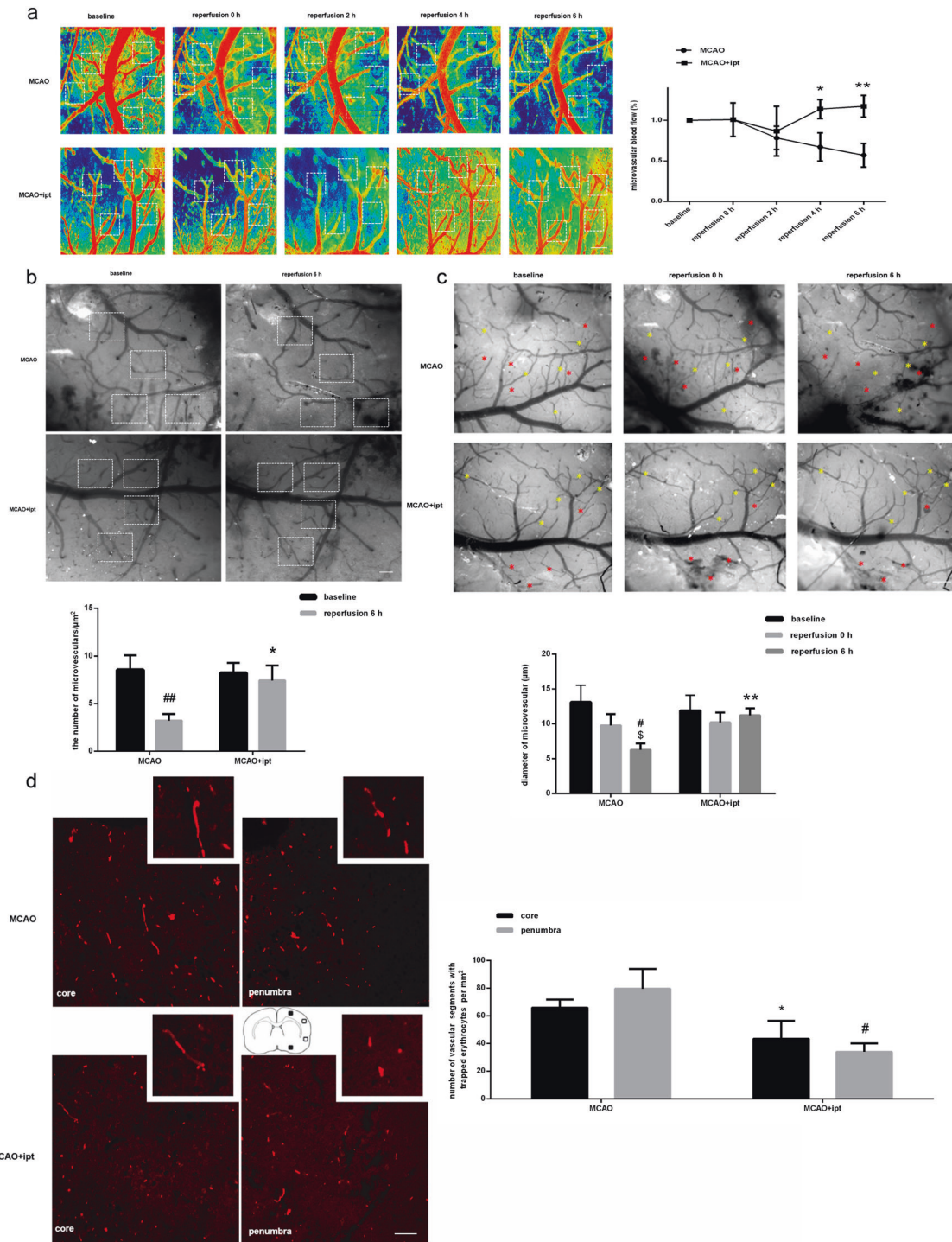


Fig. 2 Iptakalim treatment significantly improves cerebral microcirculation disorder after cerebral ischemia and reperfusion injury. a Representative images of microcirculation (left) and quantitative velocity of CBF (right) determined by a laser diode at $\lambda_3 = 830$ nm. Scale bar, 200 μm . Data are presented as mean \pm SEM, $n = 3$, $*P < 0.05$; $**P < 0.01$ vs. MCAO group. **b** Representative images (upper) and quantitative analysis of the number of microvessels in the ipsilateral (lower). Scale bar, 200 μm . Data are presented as mean \pm SEM, $n = 4$, $*P < 0.05$ vs. 6 h of reperfusion group; $##P < 0.01$ vs. baseline group. **c** Representative images of microvessels (upper) and the diameter in the ipsilateral sites (lower). Yellow, vessel diameter; red, localization of bleeding sites. Scale bar, 200 μm ; data are presented as mean \pm SEM, $n = 4$, $**P < 0.01$ vs. 6 h of reperfusion group; $^{\#}P < 0.05$ vs. baseline group; $^{\$}P < 0.05$ vs. 0 h of reperfusion group. **d** Representative fluorescent images (left) and quantification of erythrocytes (red) trapped in capillaries (right) at 6 h after reperfusion. The penumbra (■) and core (□) where erythrocytes were counted are shown in the picture. Scale bar, 100 μm ; data are presented as mean \pm SEM, $n = 5$, $*P < 0.05$ vs. core of MCAO group; $^{\#}P < 0.05$ vs. penumbra of MCAO group.

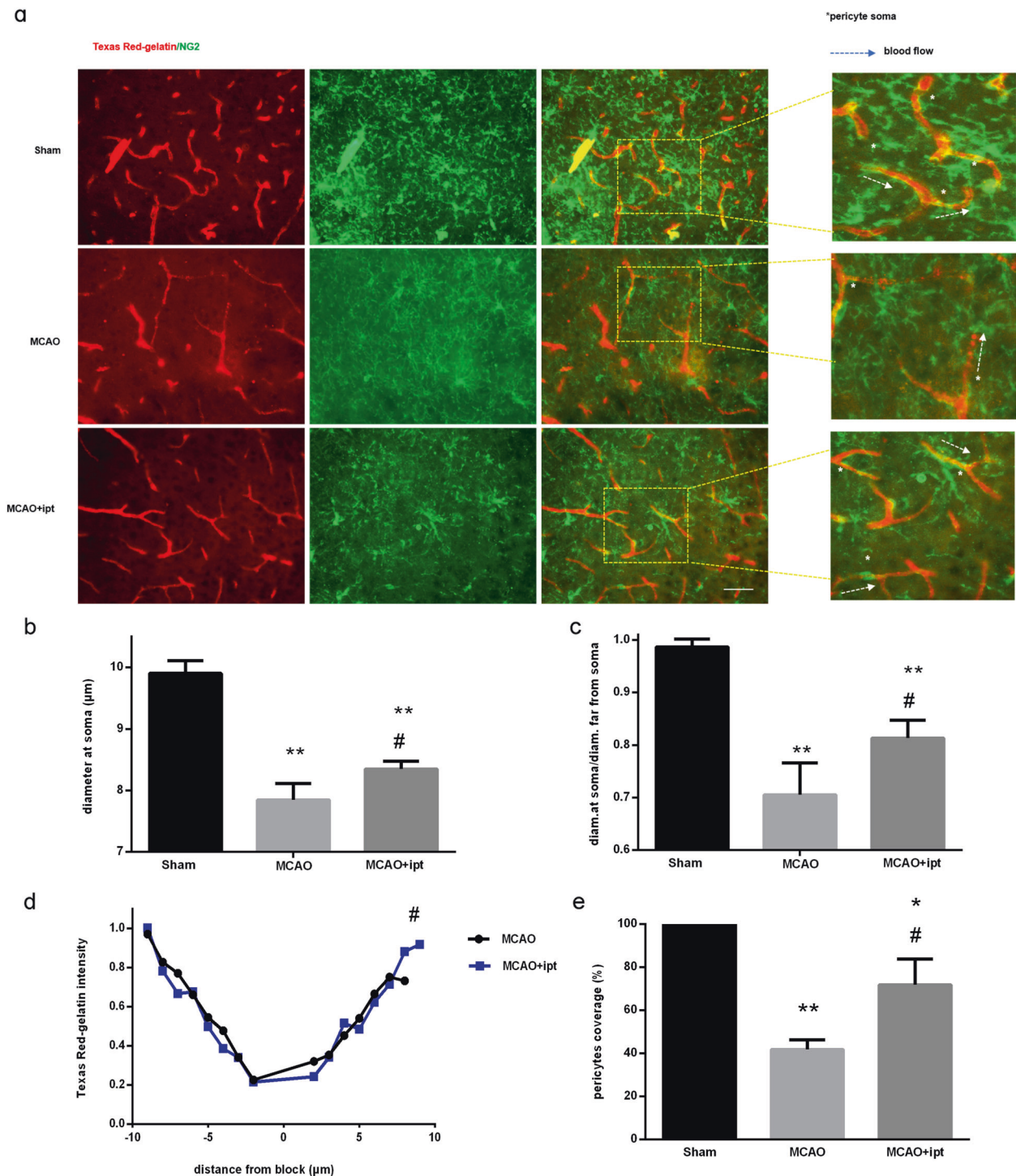


Fig. 3 Iptakalim treatment could dilate the capillaries by inhibiting the contraction of surrounding pericytes. **a** Representative images of capillaries and pericytes in the ipsilateral side after reperfusion 6 h. Texas red with gelatin (red), fully perfused capillaries; NG₂-positive cells (green), pericytes. **b** Diameter of capillaries around the pericytes soma in the ipsilateral side after reperfusion 6 h. **c** The ratio of capillary diameter from pericyte somata to the upstream of 10 μm after reperfusion 6 h. **d** The intensity of microvasculars labeled by Texas red in the ipsilateral side at 6 h after reperfusion; **e** The number of pericytes covered around the capillaries in the ipsilateral side after at 6 h of reperfusion. Scale bar, 100 μm. Data are presented as mean ± SEM, n = 5, *P < 0.05; **P < 0.01 vs. Sham group; #P < 0.05 vs. MCAO group.

intracellular calcium and ET-1. This study revealed the novel mechanisms underlying the protective effects of IPT against cerebral ischemia by restoring CBF in targeted pericytes (Scheme 1).

Recovering microcirculatory reperfusion is essential for saving penumbra after cerebral ischemia–reperfusion injury. Currently, primary therapeutic interventions are thrombolysis and surgical thrombectomy [29]; however, microcirculatory dysfunction can

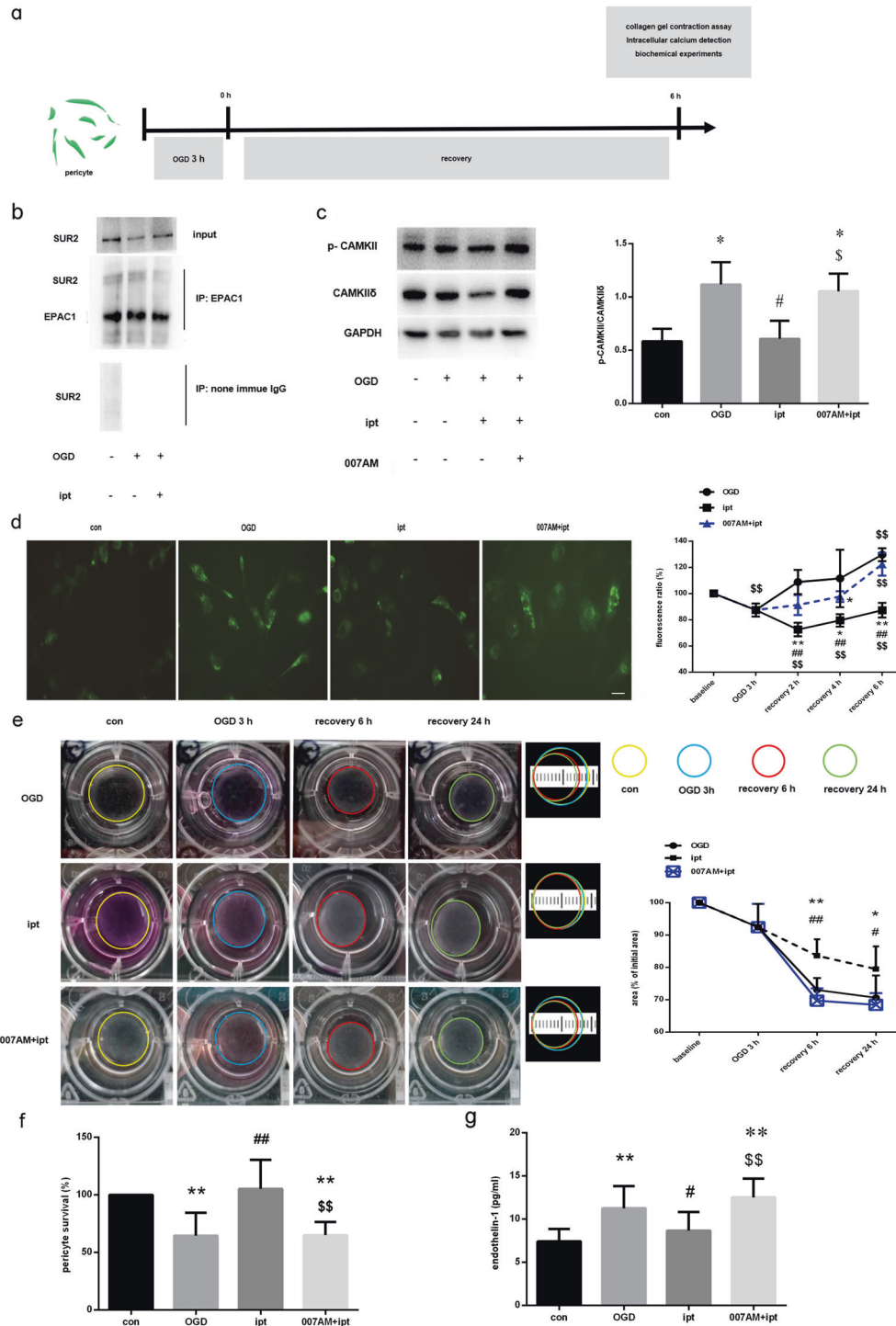


Fig. 4 Iptakalim treatment inhibits pericytes contraction by reducing formation of SUR2/EPAC1 complex, intracellular calcium and ET-1 secretion. **a** Schematic of experimental design. **b** Representative blots of SUR2/EPAC1 determined by co-immunoprecipitation. **c** Representative blots (left) and quantification (right) of phosphorylated CAMKII and CAMKII δ . Data are presented as mean \pm SEM, $n = 4$, $^*P < 0.05$, vs. con group; $^{\#}P < 0.05$ vs. OGD group; $^{\$}P < 0.05$ vs. ipt group. **d** Representative fluorescence images of Fluo 4-AM at 6 h after OGD (left) and time course of quantitative Fluo4-AM fluorescence (right). Scale bar is 50 μ m. Data are presented as mean \pm SEM, $n = 4$, $^*P < 0.05$; $^{**}P < 0.01$ vs. OGD group; $^{\#\#}P < 0.01$ vs. ipt plus 007AM group; $^{\$\$}P < 0.01$ vs. baseline group. **e** Representative images of Collagen gel contraction (left) and quantitative analysis of the area of collagen gel (right). Data are presented as mean \pm SEM, $n = 4$, $^*P < 0.05$; $^{**}P < 0.01$ vs. OGD group; $^{\#}P < 0.05$, $^{\#\#}P < 0.01$ vs. ipt plus 007AM group. **f** Cell viability detected by MTT assay at 6 h after OGD. Data are presented as mean \pm SEM, $n = 5$, $^{**}P < 0.01$ vs. con group; $^{\#}P < 0.05$; $^{\#\#}P < 0.01$ vs. OGD group; $^{\$\$}P < 0.01$ vs. ipt group. **g** Quantification of ET-1 in the culture medium of pericytes at 6 h after OGD. Data are presented as mean \pm SEM, $n = 4$, $^*P < 0.05$ vs. con group; $^{\#}P < 0.05$ vs. OGD group; $^{\$}P < 0.01$ vs. ipt group.

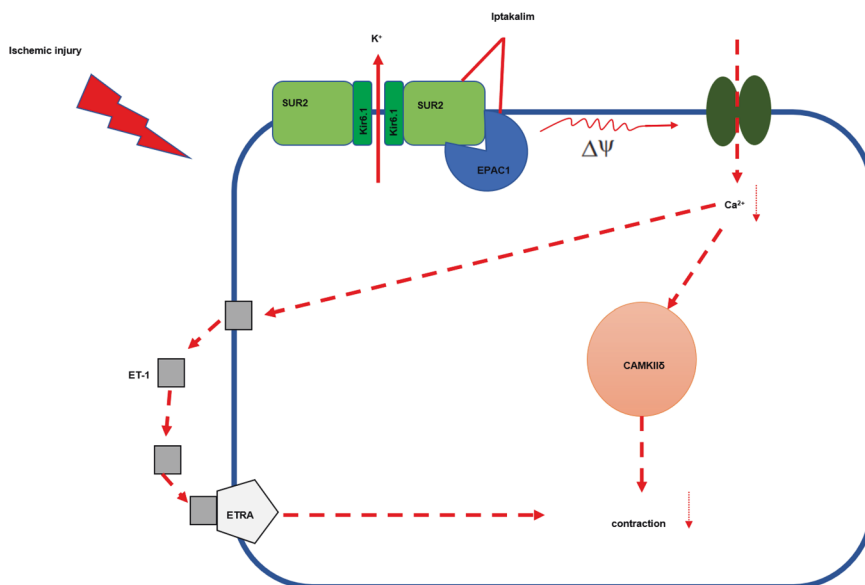
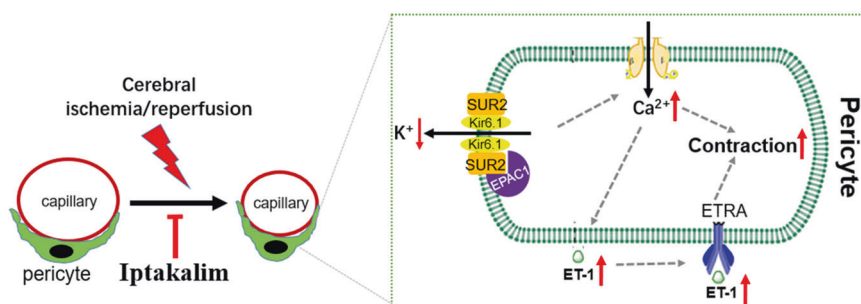


Fig. 5 Schematic diagram of iptakalim regulating pericyte contraction. Iptakalim treatment could inhibit formation of SUR2/EPAC1 complex, and thus open the K-ATP channels. K-ATP channels Opening causes hyperpolarization of the cell membrane and reduces influx of calcium, which contributes to pericyte contraction. In addition, it also reduces ET-1 secretion in pericytes and inhibits pericyte contraction.



Scheme 1 Iptakalim regulates pericyte contraction in ischemic stroke.

occur after thrombolysis and thrombectomy. Ames et al. [30] showed that no-reflow occurred after cerebral ischemia. The authors found that obstructed capillaries after ischemic insult might account for incomplete microcirculatory reperfusion [7]. It has been demonstrated that 50% of capillaries are unsuccessfully restored with the no-reflow phenomenon. Potential mechanisms of no-reflow in the brain include the following: cortical spreading depression, neurovascular uncoupling, high extracellular K⁺ concentration, and vascular dysregulation [31, 32]; edema, swollen endothelial cells, and astrocyte end-feet [33], increased permeability of the blood–brain barrier leading to the collapse of cerebral blood vessels [33, 34]; adhesion and aggregation of blood-borne elements (erythrocytes, leukocytes, and platelets), and rolling along the endothelium [35–37]; inflammatory response resulting in brain damage [8, 36]; and vasoconstriction and pericyte contraction [30, 31]. Most cerebral resistance vessels are capillaries that do not contract on their own [38]. Accumulating data have suggested that cerebral ischemia results in a decrease in capillary diameter due to significantly increased pericytes surrounding the constricted capillaries, preventing erythrocytes from passing through the narrow capillaries [39]. Recently, researchers found that pericytes are crucial for controlling the microvascular blood flow. Preclinical and clinical studies have proven that ischemia can result in capillary blood flow disorder mediated by pericyte contraction, and microvascular constrictions are independent of upstream vascular changes [27, 40]. The

contractile capacity of pericytes has been proven through in vitro and in vivo studies [27–30], and they can respond to vasoactive mediators [31–34]. Our data showed that pericytes began to contract from 3 h after OGD to 24 h of reoxygenation. We also demonstrated a significant decrease in the diameter of capillaries surrounding the pericyte somata, and pericyte coverage decreased by 56% in the penumbra at 6 h after reperfusion. Therefore, many erythrocytes were trapped in the core and penumbra, and displayed microcirculatory dysfunction at 6 h after cerebral ischemia–reperfusion. The constricted capillary leads to many trapped erythrocytes and microcirculatory dysfunction. It can also promote fibrin strand formation and platelet aggregation [39]. The lingering of red blood cells is the main cause of imbalance between oxygen demand and supply in the blood, increased capillary resistance, and capillary flow heterogeneity [41]. Our data indicate that adjusting the contraction of the pericyte may help restore CBF after cerebral ischemia–reperfusion. Although this issue is controversial for several reasons [41–43]. The first reason is that the category of pericytes is complicated. Mesh pericytes overlay the capillaries with surrounding processes, but lack smooth muscle actin [44], while precapillary sphincters, which share attributes of smooth muscle cells, are also thought to be part of the pericyte family [45]. The second reason is that upstream arterioles can control capillary blood flow, and it is not easy to distinguish them. In a recent study, Hartmann et al. [46] used cause-and-effect optical manipulations to demonstrate that

distal capillary pericytes can slowly modulate flow resistance. A small change in diameter (~20%–40%) may prevent the passage of blood cells (e.g., erythrocytes, leukocytes, and platelets) [21, 39, 40]. A small increase in diameter of 4 μm capillary is sufficient to double the velocity of red blood cells [47]; however, persistent pericyte contraction causes apoptosis, which, in turn, decreases capillary blood flow and destroys the pericyte-maintained blood–brain barrier [47, 48], all of which contribute to neuronal damage.

Calcium influx is the classic mechanism implicated in cell contraction, contributing to activating microtubules and actin filaments [49]. Myosin and α -actin are the essential proteins for the contraction and relaxation of vascular smooth muscle. Phosphorylated myosin light chain (MLC) stimulates interactions between myosin and actin, cross-bridge cycling, and ultimately cell contraction [50]. A recent study showed that α -actin-deficient pericytes can significantly decrease the diameter of capillaries [27]. Another study suggested that filamentous actins (F-actin) are the major actin in pericytes [51]. The current study demonstrated that calcium fluorescence intensity significantly increased in pericytes after OGD/R with associated upregulation of phosphorylated CAMKII. ET-1, a potent vasoconstrictor, can induce intensive vasoconstriction, acting on ETA receptors [50]. Furthermore, the abundant production of reactive oxygen species can induce the release of ET-1 and activated ETA receptor, leading to pericyte contraction [40].

We found that ET-1 released from pericytes was significantly increased after OGD/R. Previous studies have indicated that ET-1 results in vasoconstriction through protein kinase C-mediated MLC kinase phosphorylation. Activation of the phospholipase C pathway leads to diacyl-glycerol, and D-inositol-1,4,5-trisphosphate is crucial for ET-mediated transmembrane signaling. Consequently, these pathways lead to an increase in intracellular calcium. Thus, regulating calcium influx and ET-1 release are also critically important mechanisms for regulating pericyte contraction. Treatment with IPT can notably inhibit pericyte contraction after OGD/R and reduce calcium influx, thereby inhibiting ET-1 release. These data were consistent with previous studies, showing that IPT protects cardiovascular function by opening the SUR2B/Kir6.1 channel and decreasing ET-1 levels [52, 53].

IPT, a K-ATP channel opener, has been developed as an anti-hypertensive agent with high selectivity for cardiac K-ATP channels (Kir6.2/SUR2) and vascular K-ATP channels (Kir6.1/SUR2). Physiologically, opening K-ATP channels result in hyperpolarization and dilatation of microvessels [54]. IPT can easily pass through the blood–brain barrier and remain stable in the brain ($T_{\text{max}} = 30 \text{ min}$; $C_{\text{max}} = 2.25 \mu\text{g/g}$), and the IPT concentration (C_{max}) in the brain decreased by 18% after 3 h. IPT treatment (0.5–10 mg/kg per day, IP) can reduce the high locomotor activity evoked by ischemia and improve global cerebral ischemia-induced impairment of working memory [14, 15]. This study found that IPT (10 mg/kg) could inhibit pericyte contraction and improve microcirculatory dysfunction and relax capillaries. Our data showed that SUR2/Kir6.1 K-ATP channels were highly expressed in pericytes, consistent with the results from a single-cell RNA sequencing assay in a previous study [16]. Various metabolic signals can control the switch of K-ATP channels. Second messenger cAMP-dependent protein kinase phosphorylation moves the SUR2 interdomain and activates the vascular K-ATP channels [55]. EPAC is a novel downstream target of cAMP, which has two isoforms (EPAC1 and EPAC2) that play a vital role in activating the Ras-related GTPases Rap1 and Rap2 [56]. EPAC2A is an obligatory signal for sulfonylurea-induced insulin secretion in the MIN6 mouse pancreatic β cell line [57]. EPAC also influences the function of voltage-dependent calcium channels, chloride channels, sodium channels, and calcium-dependent potassium channels in various cell types [58]. EPAC forms a protein complex with other proteins [59]. Our novel finding was that EPAC1 was

abundantly expressed in pericytes and formed a complex with SUR2. While IPT reduced SUR2/EPAC1 complex formation, pretreatment with the EPAC1 agonist 007AM partially inhibited the effects of IPT. Together, the results of this study demonstrate that IPT reduces SUR2/EPAC1 complex formation to open the K-ATP channels, thereby decreasing calcium influx and ET-1 secretion, all of which contribute to the inhibition of pericyte contraction.

CONCLUSION

This study revealed that pericyte contraction caused capillary constriction and microvascular disorder in the penumbra in the acute stage of cerebral ischemia–reperfusion. IPT promoted K-ATP channel opening by reducing SUR2/EPAC1 complex formation and decreasing ET-1 release and calcium influx, thus relieving pericyte contraction and restoring microvascular blood flow. These data reveal a novel role of IPT in regulating pericyte contraction. Our findings suggest that IPT might serve as a potential regulator of pericytes for the treatment of ischemic stroke.

ACKNOWLEDGEMENTS

The National Natural Science Foundation of China (Nos. 81973301, 81773701, and 82003732), the Medical Research Project of Jiangsu Commission of Health (No. ZDA2020006), the Natural Science Foundation of the Jiangsu Higher Education Institutions of China (No. 18KJA310004), the Major Project of Nanjing Medical University (No. NMUD2018008), the Priority Academic Program Development of Jiangsu Higher Education Institutions. Thank Prof. Hai Wang for providing iptakalim in this study.

AUTHOR CONTRIBUTIONS

RBG performed the in vivo experiments. YFD mainly charged with LSI and multimodal optical imaging and revised the manuscript. ZYC, XXH, and ZY mainly participated in in vitro experiments. JY, JJ, TFX, and YQS performed the Texas Red-gelatin to the coronary microvasculature and Immunofluorescence staining. HC, XQZ obtained resources and wrote paper. XLS designed research, acquired funding, and helped to draft the paper. All authors read and approved the final paper.

ADDITIONAL INFORMATION

Supplementary information The online version contains supplementary material available at <https://doi.org/10.1038/s41401-021-00784-4>.

Competing interests: The authors declare no competing interests.

REFERENCES

1. Kloner RA, King KS, Harrington MG. No-reflow phenomenon in the heart and brain. *Am J Physiol Heart Circ Physiol.* 2018;315:H550–62.
2. Attwell D, Mishra A, Hall CN, O'Farrell FM, Dalkara T. What is a pericyte? *J Cereb Blood Flow Metab.* 2016;36:451–5.
3. Cai W, Liu H, Zhao J, Chen LY, Chen J, Lu Z, et al. Pericytes in brain injury and repair after ischemic stroke. *Transl Stroke Res.* 2017;8:107–21.
4. Cenko E, Ricci B, Kedev S, Kalpak O, Calmac L, Vasiljevic Z, et al. The no-reflow phenomenon in the young and in the elderly. *Int J Cardiol.* 2016;222:1122–8.
5. Hossmann KA. Ischemia-mediated neuronal injury. *Resuscitation.* 1993;26:225–35.
6. Rezkalla SH, Stankowski RV, Hanna J, Kloner RA. Management of no-reflow phenomenon in the catheterization laboratory. *JACC Cardiovasc Inter.* 2017;10:215–23.
7. Dalkara T, Arsava EM. Can restoring incomplete microcirculatory reperfusion improve stroke outcome after thrombolysis? *J Cereb Blood Flow Metab.* 2012;32:2091–9.
8. Yemisci M, Gursoy-Ozdemir Y, Vural A, Can A, Topalkara K, Dalkara T. Pericyte contraction induced by oxidative-nitrate stress impairs capillary reflow despite successful opening of an occluded cerebral artery. *Nat Med.* 2009;15:1031–7.
9. Yang S, Jin H, Zhu Y, Wan Y, Opoku EN, Zhu L, et al. Diverse functions and mechanisms of pericytes in ischemic stroke. *Curr Neuropharmacol.* 2017;15:892–905.

10. Armulik A, Genove G, Betsholtz C. Pericytes: developmental, physiological, and pathological perspectives, problems, and promises. *Dev Cell*. 2011;21:193–215.
11. Pan Z, Huang J, Cui W, Long C, Zhang Y, Wang H. Targeting hypertension with a new adenosine triphosphate-sensitive potassium channel opener iptakalim. *J Cardiovasc Pharmacol*. 2010;56:215–28.
12. Sikka P, Kapoor S, Bindra VK, Saini M, Saxena KK. Iptakalim: a novel multi-utility potassium channel opener. *J Pharmacol Pharmacother*. 2012;3:12–4.
13. Ran YH, Wang H. Iptakalim, an ATP-sensitive potassium channel opener, confers neuroprotection against cerebral ischemia/reperfusion injury in rats by protecting neurovascular unit cells. *J Zhejiang Univ Sci B*. 2011;12:835–45.
14. Ji J, Yan H, Chen ZZ, Zhao Z, Yang DD, Sun XL, et al. Iptakalim protects against ischemic injury by improving neurovascular unit function in the mouse brain. *Clin Exp Pharmacol Physiol*. 2015;42:766–71.
15. Chen H, Yang Y, Yao HH, Tang XC, Ding JH, Wang H, et al. Protective effects of iptakalim, a novel ATP-sensitive potassium channel opener, on global cerebral ischemia-evoked insult in gerbils. *Acta Pharmacol Sin*. 2006;27:665–72.
16. He L, Vanlandewijck M, Mae MA, Andrae J, Ando K, Del Gaudio F, et al. Single-cell RNA sequencing of mouse brain and lung vascular and vessel-associated cell types. *Sci Data*. 2018;5:180160.
17. Lu M, Yang JZ, Geng F, Ding JH, Hu G. Iptakalim confers an antidepressant effect in a chronic mild stress model of depression through regulating neuro-inflammation and neurogenesis. *Int J Neuropsychopharmacol*. 2014;17:1501–10.
18. Tamura A, Graham DL, McCulloch J, Teasdale GM. Focal cerebral ischaemia in the rat: 1. Description of technique and early neuropathological consequences following middle cerebral artery occlusion. *J Cereb Blood Flow Metab*. 1981;1:53–60.
19. Chen RL, Nagel S, Papadakis M, Bishop T, Pollard P, Ratcliffe PJ, et al. Roles of individual prolyl-4-hydroxylase isoforms in the first 24 h following transient focal cerebral ischaemia: insights from genetically modified mice. *J Physiol*. 2012;590:4079–91.
20. Gu X, Chen W, You J, Koretsky AP, Volkow ND, Pan Y, et al. Long-term optical imaging of neurovascular coupling in mouse cortex using GCaMP6f and intrinsic hemodynamic signals. *Neuroimage*. 2018;165:251–64.
21. O'Farrell FM, Mastitskaya S, Hammond-Haley M, Freitas F, Wah WR, Attwell D. Capillary pericytes mediate coronary no-reflow after myocardial ischaemia. *Elife*. 2017;6:e29280. <https://doi.org/10.7554/eLife.29280>.
22. Han X, Sun S, Sun Y, Song Q, Zhu J, Song N, et al. Small molecule-driven NLRP3 inflammation inhibition via interplay between ubiquitination and autophagy: implications for Parkinson disease. *Autophagy*. 2019;15:1860–81.
23. Liu S, Connor J, Peterson S, Shuttleworth CW, Liu KJ. Direct visualization of trapped erythrocytes in rat brain after focal ischemia and reperfusion. *J Cereb Blood Flow Metab*. 2002;22:1222–30.
24. Tigges U, Welsch-Alves JV, Boroujerdi A, Milner R. A novel and simple method for culturing pericytes from mouse brain. *Microvasc Res*. 2012;84:74–80.
25. Chen M, Zou W, Chen M, Cao L, Ding J, Xiao W, et al. Ginkgolide K promotes angiogenesis in a middle cerebral artery occlusion mouse model via activating JAK2/STAT3 pathway. *Eur J Pharmacol*. 2018;833:221–9.
26. Chamorro A. Neuroprotectants in the era of reperfusion therapy. *J Stroke*. 2018;20:197–207.
27. Alarcon-Martinez L, Yilmaz-Ozcan S, Yemisci M, Schallek J, Kilic K, Villafranca-Baughman D, et al. Retinal ischemia induces alpha-SMA-mediated capillary pericyte contraction coincident with perivascular glycogen depletion. *Acta Neuropathol Commun*. 2019;7:134.
28. Zhao K, Wen R, Wang X, Pei L, Yang Y, Shang Y, et al. EPAC inhibition of SUR1 receptor increases glutamate release and seizure vulnerability. *J Neurosci*. 2013;33:8861–5.
29. Bai J, Lyden PD. Revisiting cerebral postischemic reperfusion injury: new insights in understanding reperfusion failure, hemorrhage, and edema. *Int J Stroke*. 2015;10:143–52.
30. Ames A 3rd, Wright RL, Kowada M, Thurston JM, Majno G. Cerebral ischemia. II. The no-reflow phenomenon. *Am J Pathol*. 1968;52:437–53.
31. Ayata C, Lauritzen M. Spreading depression, spreading depolarizations, and the cerebral vasculature. *Physiol Rev*. 2015;95:953–93.
32. Hartings JA, Shuttleworth CW, Kirov SA, Ayata C, Hinzman JM, Foreman B, et al. The continuum of spreading depolarizations in acute cortical lesion development: examining Leao's legacy. *J Cereb Blood Flow Metab*. 2017;37:1571–94.
33. Garcia JH, Liu KF, Yoshida Y, Chen S, Lian J. Brain microvessels: factors altering their patency after the occlusion of a middle cerebral artery (Wistar rat). *Am J Pathol*. 1994;145:728–40.
34. Granger DN, Kvietys PR. Reperfusion therapy—what's with the obstructed, leaky and broken capillaries? *Pathophysiology*. 2017;24:213–28.
35. Mohamed Mokhtarudin MJ, Payne SJ. Mathematical model of the effect of ischemia-reperfusion on brain capillary collapse and tissue swelling. *Math Biosci*. 2015;263:111–20.
36. Fischer EG, Ames A 3d. Studies on mechanisms of impairment of cerebral circulation following ischemia: effect of hemodilution and perfusion pressure. *Stroke*. 1972;3:538–42.
37. Ritter LS, Orozco JA, Coull BM, McDonagh PF, Rosenblum WI. Leukocyte accumulation and hemodynamic changes in the cerebral microcirculation during early reperfusion after stroke. *Stroke*. 2000;31:1153–61.
38. Gould IG, Tsai P, Kleinfeld D, Linninger A. The capillary bed offers the largest hemodynamic resistance to the cortical blood supply. *J Cereb Blood Flow Metab*. 2017;37:52–68.
39. Peppiatt CM, Howarth C, Mobbs P, Attwell D. Bidirectional control of CNS capillary diameter by pericytes. *Nature*. 2006;443:700–4.
40. Nortley R, Korte N, Izquierdo P, Hirunpattarasilp C, Mishra A, Jaunmuktane Z, et al. Amyloid beta oligomers constrict human capillaries in Alzheimer's disease via signaling to pericytes. *Science*. 2019;365:eaav9518.
41. Hossmann KA. Pathophysiology and therapy of experimental stroke. *Cell Mol Neurobiol*. 2006;26:1057–83.
42. Li Y, Lucas-Osma AM, Black S, Bandet MV, Stephens MJ, Vavrek R, et al. Pericytes impair capillary blood flow and motor function after chronic spinal cord injury. *Nat Med*. 2017;23:733–41.
43. Wang YL, Wang XH, Liu YL, Kong XQ, Wang LX. Cardiac lymphatic obstruction impairs left ventricular function and increases plasma endothelin-1 and angiotensin II in rabbits. *Lymphology*. 2009;42:182–7.
44. Grant RI, Hartmann DA, Underly RG, Berthiaume AA, Bhat NR, Shih AY. Organizational hierarchy and structural diversity of microvascular pericytes in adult mouse cortex. *J Cereb Blood Flow Metab*. 2019;39:411–25.
45. Grubb S, Cai C, Hald BO, Khenouf L, Murmu RP, Jensen AGK, et al. Precapillary sphincters maintain perfusion in the cerebral cortex. *Nat Commun*. 2020;11:395.
46. Hartmann DA, Berthiaume AA, Grant RI, Harrill SA, Koski T, Tieu T, et al. Brain capillary pericytes exert a substantial but slow influence on blood flow. *Nat Neurosci*. 2012;24:633–45.
47. Rungta RL, Chaigneau E, Osmanski BF, Charpak S. Vascular compartmentalization of functional hyperemia from the synapse to the Pia. *Neuron*. 2018;99:362–75.e4.
48. Hauck EF, Apostel S, Hoffmann JF, Heimann A, Kempfski O. Capillary flow and diameter changes during reperfusion after global cerebral ischemia studied by intravital video microscopy. *J Cereb Blood Flow Metab*. 2004;24:383–91.
49. Burdyla T, Borysova L. Ca²⁺ signalling in pericytes. *Adv Exp Med Biol*. 2018;1109:95–109.
50. Ikebe M, Hartshorne DJ. The role of myosin phosphorylation in the contraction-relaxation cycle of smooth muscle. *Experientia*. 1985;41:1006–10.
51. Kureli G, Yilmaz-Ozcan S, Erdener SE, Donmez-Demir B, Yemisci M, Karatas H, et al. F-actin polymerization contributes to pericyte contractility in retinal capillaries. *Exp Neurol*. 2020;332:113392.
52. Wang S, Guo X, Long CL, Li C, Zhang YF, Wang J, et al. SUR2B/Kir6.1 channel openers correct endothelial dysfunction in chronic heart failure via the miR-1-3p/ET-1 pathway. *Biomed Pharmacother*. 2019;110:431–9.
53. Gao M, Wang Y, Wang H. Effects of iptakalim on intracellular calcium concentrations, PKA and PKC activities in rat tail artery smooth muscle cells. *Yao Xue Xue Bao*. 2005;40:954–7.
54. Hosford PS, Christie IN, Niranjana A, Aziz Q, Anderson N, Ang R, et al. A critical role for the ATP-sensitive potassium channel subunit KIR6.1 in the control of cerebral blood flow. *J Cereb Blood Flow Metab*. 2019;39:2089–95.
55. Kang G, Leech CA, Chepurny OG, Coetzee WA, Holz GG. Role of the cAMP sensor Epac as a determinant of KATP channel ATP sensitivity in human pancreatic beta-cells and rat INS-1 cells. *J Physiol*. 2008;586:1307–19.
56. Roberts OL, Dart C. cAMP signalling in the vasculature: the role of Epac (exchange protein directly activated by cAMP). *Biochem Soc Trans*. 2014;42:89–97.
57. Shibasaki T, Takahashi T, Takahashi H, Seino S. Cooperation between cAMP signalling and sulfonyleurea in insulin secretion. *Diabetes Obes Metab*. 2014;16 Suppl 1:118–25.
58. Manoury B, Idres S, Leblais V, Fischmeister R. Ion channels as effectors of cyclic nucleotide pathways: Functional relevance for arterial tone regulation. *Pharmacol Ther*. 2020;209:107499.
59. Aromataris EC, Roberts ML, Barritt GJ, Rychkov GY. Glucagon activates Ca²⁺ and Cl⁻ channels in rat hepatocytes. *J Physiol*. 2006;573:611–25.